Journal of Electroceramics 1:2, 125–132, 1997

Impedance and Modulus Spectroscopy of ZnO Varistors

M. ANDRES-VERGES & A.R. WEST

Depto. Quimica Inorganica, Universidad de Extremadura, Avda, Elvas s/n. 06071-Badajoz, Spain
University of Aberdeen, Department of Chemistry, Meston Walk, Aberdeen AB24 3UE

Submitted June 20, 1996; Revised February 19, 1997; Accepted April 3, 1997

Abstract. The ac response of ZnO varistors has been investigated over the temperature range 100 to 380°C using impedance and modulus spectroscopy. Impedance spectra show only a single peak, which represents the most resistive component in the sample and is responsible for the dc properties, whereas an additional peak appears in the modulus spectrum. The two components have temperature-dependent activation energies in the ranges, 0.52–1.00 and 0.54–0.64 eV, respectively but their resistances differ by 1 to 2 orders of magnitude. From their capacitance values, each represents a region ~100 to 500 Å thick; they are tentatively assigned to an electrically-active interface and an intergranular layer.

Keywords: zinc oxide varistors, impedance and modulus spectroscopy, impedance data, equivalent circuit analysis, ZnO, dc and ac conductivity

Introduction

ZnO ceramics containing Bi_2O_3 and other metal oxides, principally Sb_2O_3, CoO and MnO, are characterized by highly non-linear voltage-current behavior. The non-linear properties of such materials, known as metal oxide varistors, MOV, are closely related to their microstructure. There has, however, been much debate as to the mechanism of varistor action and the microstructural features that give rise to this. ZnO varistors are electrically heterogeneous and may contain several phases; as well as ZnO, these include a spinel (''$Zn_7Sb_2O_{12}$'') and Bi_2O_3 which can dissolve several metal oxides [1,2]. The surface of the ZnO grains at ZnO-ZnO contacts may contain bismuth to a depth of 20–25 Å. In addition, much thicker grain boundary regions, composed of a bismuth-rich phase may also be present [3–7].

At the ZnO-ZnO grain boundaries, double Schottky barriers and their associated depletion regions are believed to exist and these are held responsible for the non-linear behavior [8–10]. The Schottky barriers arise from electron traps located in the region of the grain boundaries; these traps have been characterized by various techniques including deep level transient spectroscopy, DLTS and capacitance transient spectroscopy, CTS and are located at various energy levels in the range 0.6–0.97 eV [11–15]. Traps at energy levels less than 0.5 eV have been assigned to the depletion region [16–18]. If, as supposed, the Schottky barriers arise at the interface between ZnO grains, then the question arises as to the role of the Bi_2O_3-rich region in the electrical properties. Studies carried out by several groups [19,20] appear to show that Bi_2O_3 plays an important role in the overall electrical properties of ZnO-based varistors: leakage current, non-linearity coefficient α, capacitance values, degradation phenomena. However, the mechanism responsible for this behavior is at present unclear.

Impedance spectroscopy is a powerful technique for the characterization of grain boundaries in ceramic materials. It has the great advantage over dc techniques of being able to separate the electrical response of different regions of a ceramic, provided their electrical responses are within the measuring range of the instrumentation and the time constants (given by the product of resistance, R and capacitance, C) of the various regions differ by more than about one decade. There is considerable versatility, and

complexity, in the analysis of ac data because the data can be analyzed in any of four interrelated basic formalisms: the impedance, admittance, electric modulus and permittivity [21,22]. The use of combined impedance and modulus spectroscopic plots is particularly useful for separating components with, for example, similar resistances but different capacitances or vice versa, similar capacitances with dissimilar resistances. Thus, in cases where one of the components is much more resistive than the other(s), it dominates the impedance response whereas the components that are seen most clearly in the modulus response are those with the smallest capacitance values. In the present work, we find that the electrical make-up of ZnO varistors is complex and that combined impedance and modulus spectroscopy is a much more powerful method than impedance analysis alone for separating and characterizing the various electrical components. In addition, phenomena are shown up in the modulus plots that remain hidden in impedance plots.

Experimental

Commercial ZnO varistors operating at 220 V were provided by Bowthorpe Thermometrics. The varistors with Al electrodes were attached to the Pt leads of a conductivity jig which was placed inside a horizontal tube furnace whose temperature was controlled and measured to $\pm 3^{\circ}$C. The furnace and jig were allowed to equilibrate at each temperature for 30 mins prior to impedance measurements. Small amplitude, two terminal ac impedance measurements were made over the frequency range 10^{-2} Hz to 10^{6} Hz using a combination of Solartron 1250/1286 and Hewlett-Packard 4192 instrumentation. In a second set of experiments, the Al electrodes were removed, the pellet surfaces polished and fresh electrodes of In/Ga alloy applied in a conventional 2-terminal configuration. All conductivity data reported here were reversible on heat-cool-heat cycles.

X-ray diffraction patterns recorded using a Philips diffractometer, CuKα, radiation, showed the presence of three principal phases: ZnO, a spinel phase whose XRD pattern was similar to that of $Zn_7Sb_2O_{12}$ [23] and a phase whose XRD pattern was similar to $Bi_{24}CoO_{37}$ [24].

Results

Impedance measurements on the as-received, electroded varistors were made in air over the temperature range 100 to 380°C on the heating cycle. A typical impedance complex plane plot, Z'' vs. Z', is shown in Fig. 1; it contains a single arc. At higher temperatures, this arc had a non-zero, high frequency intercept (not shown). Typical high frequency intercept values were $\sim 50\,\Omega$ but since, at high frequencies, the data were influenced by inductive effects associated with the experimental arrangement, care was needed in order to obtain meaningful resistance values from the high frequency intercept. Inductive effects generally lead to an overestimate of resistance value and so the true high frequency resistance value should be significantly lower than $50\,\Omega$. This small resistance value, labeled R_3, is attributed to the core of the semiconducting ZnO grains, in accordance with the generally-accepted view. Further analysis of this region has not been attempted.

The low frequency intercept of the impedance arc represents the total resistance R_T, of the sample. It has values decreasing from $\sim 10^8$ to $10^3\,\Omega$ with increasing temperature over the range 100 to 380°C. There is no indication of any additional low frequency features in the impedance data and therefore, R_T represents the dc resistance of the sample. Although the impedance complex plane plots showed a single arc, indicative of a single parallel *RC* component, which is consistent with the results reported by other groups [25–28], further data analysis revealed a more complex electrical make-up of the sample. The *same data* as used in Fig. 1 are shown in Fig. 2, but replotted in the electric modulus complex plane, M'' vs. M'. Two almost equal-sized arcs are now seen, in contrast to

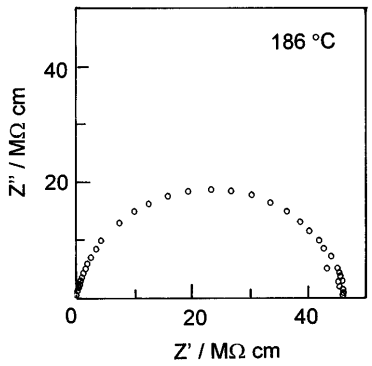

Fig. 1. Impedance complex plane plot (10^{-2} Hz $< f < 10^{4}$ Hz) of a commercial varistor at 186°C.

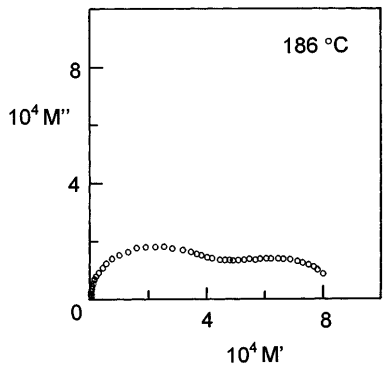

Fig. 2. Electric modulus complex plane plot for the same data set as used in Fig. 1.

the single semicircle seen in the complex impedance plane. This indicates the presence of two parallel *RC* elements of similar capacitance. (The diameter of semicircles in the M'' vs. M' plane is inversely proportional to capacitance.)

The contrasting information obtained from Z^* and M^* plots, Figs. 1 and 2, may be better understood by comparing M'' and Z'' spectroscopic plots, Fig. 3: the Z'' spectrum shows one peak but the M'' spectrum shows two peaks. The single Z'' peak corresponds to the lower frequency M'' peak; this element is the most resistive by far and dominates the overall sample resistance at all temperatures studied. The associated resistance of the high frequency M'' peak is too small for it to be detected easily in the Z'' spectroscopic plot.

In order to interpret the results shown in Figs. 1–3, it is necessary to propose an equivalent circuit so as to be able to extract resistance and capacitance values for the different components. The most frequently-used circuit with electrical ceramics, in which the current follows a series-connected pathway through grains and grain boundaries, is a series combination of

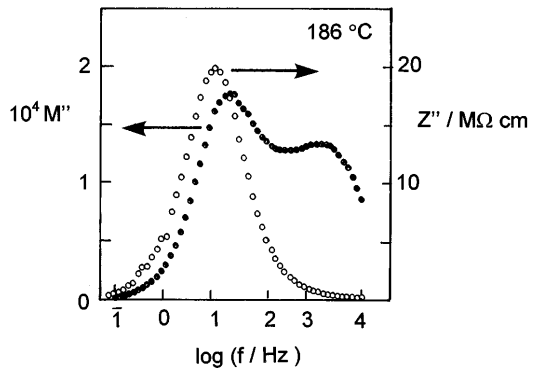

Fig. 3. Impedance Z'' amd modulus M'' spectroscopic plots for the same data set as used in Figs. 1 and 2.

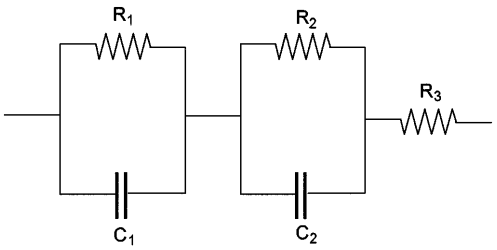

Fig. 4. Equivalent circuit used to represent the high temperature response.

parallel *RC* elements; an appropriate circuit for the present materials is shown in Fig. 4 and has also been proposed previously for ZnO varistors [28–31]. The impedance, Z^*, of this circuit is given by

$$Z^* = \left[\frac{1}{R_1} + j\omega C_1\right]^{-1} + \left[\frac{1}{R_2} + j\omega C_2\right]^{-1} + R_3$$

$$= \frac{R_1}{1 + (\omega R_1 C_1)^2} + \frac{R_2}{1 + (\omega R_2 C_2)^2}$$

$$+ R_3 - j\left[R_1 \frac{\omega R_1 C_1}{1 + (\omega R_1 C_1)^2} + R_2 \frac{\omega R_2 C_2}{1 + (\omega R_2 C_2)^2}\right]$$

The electric modulus, M^*, is given by

$$M^* = j\omega C_0 Z^*$$

$$= \frac{\omega Co R_1 \cdot \omega R_1 C_1}{1 + (\omega R_1 C_1)^2} + \frac{\omega Co R_2 \cdot \omega R_2 C_2}{1 + (\omega R_2 C_2)^2}$$

$$+ j\left[\frac{Co}{C_1} \cdot \frac{\omega R_1 C_1}{1 + (\omega R_1 C_1)^2}\right.$$

$$\left. + \frac{Co}{C_2} \cdot \frac{\omega R_2 C_2}{1 + (\omega R_2 C_2)^2} + \omega Co R_3\right]$$

The term $\omega RC/1 + (\omega RC)^2$, in the imaginary parts of both Z'' and M'' is responsible for Debye-like peak shapes in spectroscopic plots, i.e. Z'', M'' vs. $\log f$; as can be seen, the Z'' peaks are scaled by R whereas the M'' peaks are scaled by Co/C; Co is the vacuum capacitance of the cell, without the sample and is equal to $e_o A \ell^{-1}$ where e_o is the permittivity of free space, A is the area and ℓ the thickness of the space occupied by the sample.

By application of this circuit to the present materials, element R_1C_1 is assigned to the most resistive element which dominates the impedance results, R_2C_2 to the high frequency M'' peak and R_3 to the conductive core of the ZnO grains: there should also be a capacitance C_3 in parallel with R_3 that

represents the bulk capacitance of the grains but frequencies much higher than those available would be needed to determine the value of C_3. Values of R_1, R_2, C_1 and C_2 were obtained from the spectroscopic plots, as follows. R_1 was obtained directly from the Z'' spectroscopic plot since, at the peak maximum $Z''_{max} = R_1/2$. R_2 was obtained from the maximum of the high frequency M'' peak using the relation $2\pi f_{max} R_2 C_2 = 1$; C_2 was obtained from the height of the M'' peak at which $M''_{max} = C_0/2C_2$. C_1 was obtained similarly from the low frequency M'' peak. Values of R_1 and R_2 as a function of temperature are summarized in Arrhenius conductivity format in Fig. 5. Capacitance values are listed in Table 1.

The temperature dependences of R_1 and R_2 show considerable complexity, Fig. 5. Both show curvature in the Arrhenius plots and a trend towards a lower and perhaps constant activation energy of 0.52 to 0.54 eV below about 150°C. Around 300°C, the data for R_2 appear to show a small, but reproducible discontinuity.

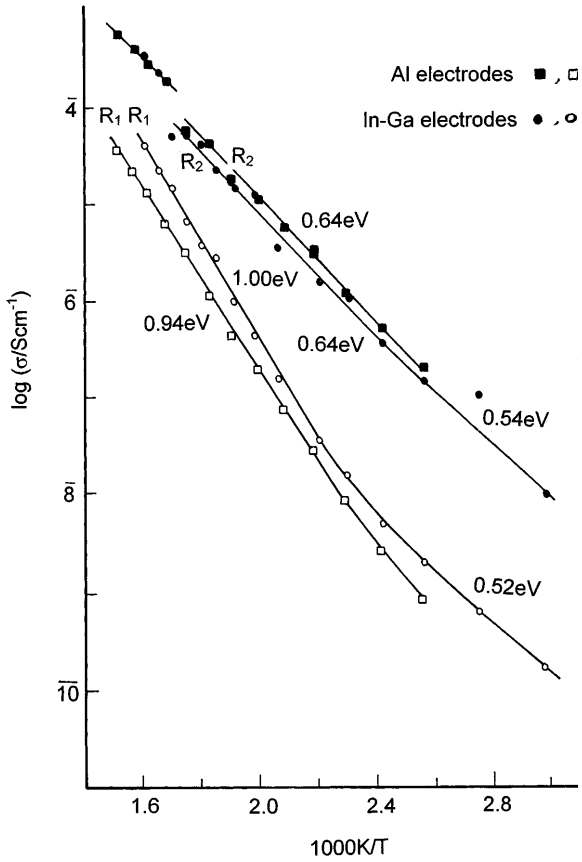

Fig. 5. Arrhenius plots for resistances R_1 and R_2.

Table 1. Capacitance Values (pF cm^{-1})

Electrode	C_1	C_2(<250°C)	(>250°C)
Al	175	227	202
In/Ga	168	198	172

On comparing the results obtained with the two sets of electrodes, Al and In/Ga, the R_2 data, including the discontinuity at ~300°C, are seen to be essentially independent of the electrodes used but the R_1 data show significant differences. Thus, while the occurrence of both resistances R_1 and R_2 is clearly sample-related rather than being associated with the electrode-sample interfaces, resistance R_1 is, somehow, affected by either the nature of the electrodes or the procedures associated with attaching the electrodes. It has been reported [32] that varistor action is critically dependent on the presence of excess oxygen (as well as Bi) at the ZnO-ZnO interfaces with activation energies varying from 0.6 to 1.0 eV with variation in oxygen content; the differences in R_1 seen for the two electrode types may also be associated with variations in oxygen content caused by the different procedures used to electrode the samples.

To further investigate any dependence of R_1 and R_2 on atmosphere, a varistor sample, was heated in 1 bar O_2 at 1200°C for 30 mins, cooled in the same atmosphere at 2°C min^{-1} and impedance data remeasured on a stepwise heating cycle, as previously. The impedance and modulus plots had very similar general appearance before and after the oxygen anneals. Arrhenius plots for the two resistances are shown in Fig. 6; whilst R_2 was essentially unaffected by the oxygen anneals, R_1 increased by a factor of 2–3 at all temperatures. Hence, absorption of oxygen occurs in the region responsible for R_2. Presumably, this leads to an decrease in carrier concentration since the conductivity decreases.

The capacitance data, Table 1 show that, to a first approximation, C_1 and C_2 have similar values, in the range 170–220 pF cm^{-1}. Assuming that the regions responsible for C_1 and C_2 have typical high frequency permittivities of ~10 corresponding to capacitances of ~ 1 pF cm^{-1} per unit volume, then C_1 and C_2 each represent regions occupying in total about 0.5% of the volume of the samples. Assuming the ''brickwork model'' for the varistor microstructure, in which grains and grain boundaries are electrically in series, and an average size of the ZnO grains of 10 μm, then the grain boundary/interfacial regions responsible for

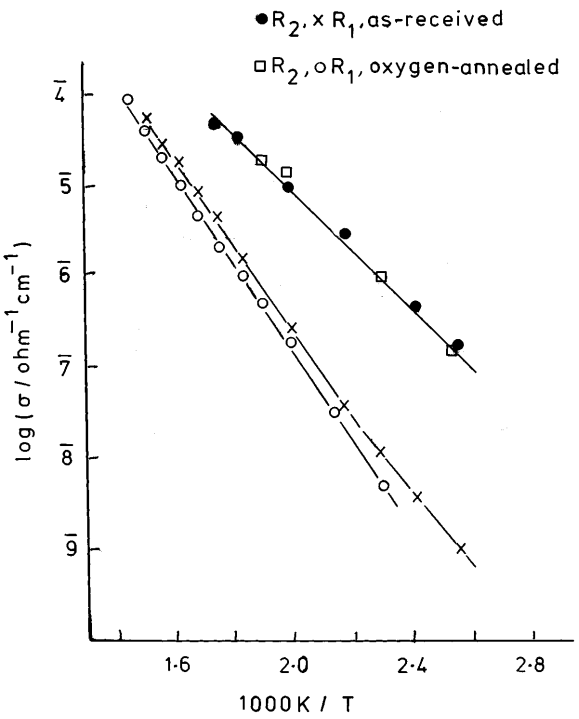

Fig. 6. Arrhenius plots for varistors: a) as-received, b) heated at 1200°C in O_2.

C_1 and C_2 have thicknesses of $\sim 0.05\,\mu m = 500$ Å. These values are larger than expected for the grain boundaries in well-sintered ceramics; they are also larger than the thicknesses, ~20 Å, of the Bi-rich regions that are believed to form at all of the ZnO-ZnO interfaces, but they are comparable to the thicknesses suggested for the depletion layers [4,6,7,32].

The data for C_2, Table 1, show a discontinuity at ~ 250°C. This is seen with both sets of electrodes and was reversible on heating/cooling cycles. The origin of this effect is not known; it could be associated with oxygen uptake/desorption and an associated variation in the thickness of the regions responsible for element R_2C_2 or it could signal a change in conduction pathway through the sample; it occurs at approximately the same temperature as the discontinuity in R_2, Fig. 5.

Discussion

The results presented above concern the impedance response of varistors at elevated temperatures, ≥ 100°C. At these temperatures at least, the materials are electrically heterogeneous. Three regions are apparent; one appears to be the highly conducting grain cores and is not considered further. The other two are of roughly comparable thickness, judging from their similar order-of magnitude capacitance values, but differ in their resistances by 1–2 orders of magnitude, depending on temperature; from the capacitance values, each occupies about 0.5% of the volume of the varistor sample.

The presence of these two components is clearly seen in the electric modulus formalism of data analysis because the size of the M'' spectroscopic peaks and the M'' vs. M' semicircles is inversely proportional to the capacitance of each component. By contrast, only the more resistive of the two components is seen in the impedance plots, for the simple reason that the size of Z'' peaks and Z'' vs. Z' semicircles is proportional to R; thus, the impedance of component R_2C_2 is effectively hidden under the high frequency response of component R_1C_1.

Similar impedance responses, with a single semicircle have been reported previously in ZnO varistors, leading to their interpretation in terms of a single parallel *RC* element in series with the grain core resistance. The results presented here indicate, for these varistors at least, a more complex electrical microstructure. They also demonstrate the importance of making a more comprehensive data analysis than is obtained by use of a single formalism, such as the impedance, alone.

At this stage, we have not, of course, *proved* that the series-connected array of parallel *RC* elements, Fig. 4, is the correct representation of the sample. It is always possible to find >1 equivalent circuit to represent a given ac response; in the present case, a circuit made up of a parallel array of series-connected *RC* elements such as suggested previously [17] could also give rise to the observed response at high frequencies. However, such a circuit, with series capacitances, would not permit dc conduction through the sample and additional features in the impedance response at low frequencies would be expected; there was no evidence for such additional low frequency effects. Absolute proof that a particular circuit is correct is usually impossible; instead, circumstantial evidence is needed to show the probable correctness of a proposed circuit. The circuit adopted here is that used to represent the electrical properties of a wide range of electrical ceramics, especially at frequencies that are towards the lower end of the ac spectrum, as

the response approaches the limiting dc response. Hence, resistance R_1 is largely responsible for the dc resistance of the varistor sample; as seen from Fig. 5, its value at 150°C, is $\sim 10^8$ ohm, consistent with the behavior expected of a reasonably good insulator. R_2 also is a large resistance, $\sim 10^6$ ohm at 150°C, although small by comparison with R_1.

The activation energies for R_1 and R_2 are close to the values reported by several researchers for grain boundary electron traps, as summarized in Table 2. These interfacial electron traps are likely to be located at either ZnO-ZnO grain-boundary interfaces (homojunctions) or at ZnO-Bi_2O_3-ZnO interfaces (heterojunctions). However, such traps are likely to be involved in the dc conduction pathway, rather than simply being part of dipolar elements that are in parallel with the dc conduction. The traps therefore provide the activation barrier to be overcome in dc conduction. These results contrast with those obtained by low temperature capacitance and admittance complex plane analysis and DLTS, for which activation energies in the range 0.15 to 0.50 eV were observed [16,17] and interpreted in terms of a parallel array of series *RC* circuit elements [17]: any such series-connected *RC* elements may correspond to localized or ac conductivity, but cannot form part of a dc pathway.

The Arrhenius conductivity plots for R_1 and R_2, Fig. 5 both show clear evidence of curvature, with a tendency to limiting lower activation energies, ~ 0.53 eV, at lower temperatures. The curvature in the Arrhenius plots may then represent a distribution in trap levels or barrier heights in the dc conduction pathway; at the lowest temperatures, only those electrons in the most shallow traps are able to contribute to the conductivity but, with increasing temperature, the carrier concentration rises as electrons from increasingly deeper traps become activated.

Table 2. Summary of grain interface electron traps for ZnO varistors

Author	Method	E_a(ev)	Reference
Tsuda et al.	DLTS	0.94	[11]
Winston et al.	DLTS	0.97	[12]
Gambino et al.	CTS	0.60–0.70	[13]
Maeda et al.	ICTS[a]	0.60	[14]
Yano et al.	DLTS	0.65	[15]
This study	IS[b]	0.97, 0.64	

[a] ICTS: Isothermal capacitance transient spectroscopy.
[b] IS: Impedance spectroscopy.

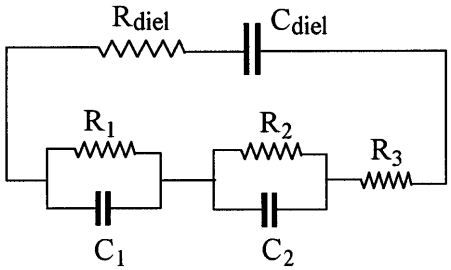

Fig. 7. Equivalent circuit used to represent the combined high and low temperature response.

By combination of the high temperature results reported here and the low temperature literature results, a more comprehensive idealized equivalent circuit is proposed, Fig. 7. It has the same series-connected elements as Fig. 4 to represent the dc properties; these are in parallel with the low temperature dielectric or ac response. This circuit is simplified/idealized in that

i) there may be >1 dielectric element in parallel with the dc component;
ii) the nature of the dc component may change with temperature.

Nevertheless, it serves to demonstrate that both dielectric (series *RC* elements)- and dc (parallel *RC* elements)-connected components are needed to explain the complete response of ZnO varistors.

There is only limited understanding of the relationship between the properties and distribution of microjunctions and the global behavior of the random networks in macroscopic varistors. Thus, we have no direct information on the nature of the regions that are responsible for R_1, R_2, and can only tentatively assign these components to different regions of the microstructure. It is likely that they are associated with the interfacial region between ZnO grains but there seem to be at least two diametrically opposed possibilities i.e. that R_1C_1 is associated with either the homojunctions or the heterojunctions (and vice versa for R_2C_2).

Following Einzinger [19], who found that the leakage current across a Bi-rich intergranular layer was much larger than that across a direct ZnO-ZnO contact that did not have the intergranular phase, it could be possible to assign R_1C_1 and R_2C_2 to the junctions ZnO-ZnO (homojunction) and ZnO-Bi phase-ZnO (heterojunction), respectively. This conclusion is also partially supported by other researchers

who have tentatively attributed a DLTS signal at 0.94 eV to a ZnO-ZnO grain-boundary interface [11] and a DLTS signal at 0.65 eV to a ZnO/PrCoOx/ZnO junction [15]. Against this, however, it has been calculated that, whilst homojunctions do exist, their associated energy barrier is no greater than 0.1 eV and therefore, they cannot be responsible for varistor action [33].

An alternative explanation could be that R_1C_1 represents the heterojunctions, specifically those in which the ZnO grain surfaces contain a thin layer of excess Bi and O; this is consistent with the observation that such interfaces are necessary for varistor action to be observed [32]. However, there would still remain the question as to the origin of R_2; given that its activation energy is $\gg 0.1$ eV, it would appear not to be associated with homojunctions [33].

The electrical nonuniformity of the grain boundaries within ZnO varistors has been discussed by several researchers [34–37]. Bartkowiak et al. [34] classified grain boundaries into ''good'', ''bad'' and ''ohmic'' junctions. Good junctions or varistor-active grain boundaries have high leakage resistance and high coefficient of nonlinearity and appear to contain a small excess of bismuth and oxygen, just sufficient to cover each grain with approximately a monolayer of both elements. It was shown as well, that the barrier height $\varnothing_B$ depends on the amount of excess oxygen at the grain boundary, and can vary between 1 and 0.65 eV for coverages of between >1 monolayer and approximately zero monolayer, respectively. If we consider that Bi is present on the grain boundary to a depth of 20–25 Å, the bad junctions might be associated with a deficiency of oxygen. Homojunctions ZnO-ZnO without any Bi [19], are not considered within this type of junction; their associated energy barrier is calculated to be no greater than 0.1 eV and therefore, they can not be responsible for varistor action [33].

From the similarity in activation energies for R_2 and junctions without oxygen and also for R_1 and junctions with one monolayer of excess of oxygen, it could be possible to assign R_1C_1 and R_2C_2 to good and bad junctions, respectively. Consistent with this, good and bad junctions would have resistances which differ by several orders of magnitude, as found here for R_1 and R_2. These assignments do not, however, match the observations, Fig. 6, that R_1, but not R_2 is affected by heating the sample in an oxygen-rich atmosphere.

Our current feeling is that the R_2C_2 component may be associated with a Bi-rich intergranular layer, consistent with Einzinger's observations [19] and with a similarity in activation energy for R_2 and Bi_2O_3 of between 0.56 and 0.66 eV [20]. In this case, the intergranular layer would represent part of the pathway for the flow of current through the device and be in series with the Schottky barriers, characterized by resistance R_1, associated with active grain boundaries. This part of the pathway would be equivalent to the ohmic junctions in agreement with data reported by several researchers [36,38].

Conclusions

Previous studies on the ac response of ZnO varistors have been confined to low temperatures; in many of these, localized conductivity associated with a range of trap states has been studied, rather than long-range dc conduction. In the present study, by contrast, the electrical properties at higher temperature are measured and these correspond to dc conduction characteristics. From the combined impedance and modulus method of data analysis, two components are in evidence. These components appear to be in series since they represent dc conduction through the sample: if they were instead attributable to localized conductivity hops, the associated series-connected capacitances would not permit dc conduction and would be immediately apparent in the impedance plots. One of the resistances, R_1, is sensitive to oxygen pressure and is assigned to an electrically-active interface which is influenced by oxygen absorption/desorption. The other, R_2, is attributed to an intergranular phase.

References

1. M. Inada, *Jpn. J. Appl. Phys.*, **17**, 1 (1978).
2. M. Inada, *Jpn. J. Appl. Phys.*, **17**, 673 (1978).
3. D.R. Clarke, *J. Appl. Phys.*, **49**, 2407 (1978).
4. D.R. Clarke, *J. Appl. Phys.*, **50**, 6829 (1979).
5. W.D. Kingery, J.B. Vander Sande and T. Mitamura, *J. Am. Ceram. Soc.*, **62**, 22 (1979).
6. W.G. Morris, *J. Vac. Sci. Tech.*, **13**, 926 (1976).
7. A.T. Santhanam, T.K. Gupta and W.G. Carlson, *J. Appl. Phys.*, **50**, 852 (1979).
8. P.R. Emtage, *J. Appl. Phys.*, **48**, 4372 (1977).
9. K. Eda, *J. Appl. Phys.*, **49**, 2964 (1978).
10. P.L. Hower and T.K. Gupta, *J. Appl. Phys.*, **50**, 4847 (1979).

11. K. Tsuda and K. Mukae, in *High Tech. Ceramics*, edited by P. Vincenzini (Elsevier, Amsterdam, 1987), pp. 1781–90.
12. R.A. Winston and J.F. Cordaro, *J. Appl. Phys.*, **68**, 6495 (1990).
13. J.P. Gambino, W.D. Kingery, G.E. Pike, H.R. Philipp and L.M. Levinson, *J. Appl. Phys.*, **61**, 2571 (1987).
14. T. Maeda, S. Meguro and M. Takata, *Jpn. J. Appl. Phys.*, **28**, L714 (1989).
15. Y. Yano, Y. Takai and H. Morooka, *J. Mater. Res.*, **9**, 112 (1994).
16. J.F. Cordaro, Y. Shim and J.E. May, *J. Appl. Phys.*, **60**, 4186 (1986).
17. M.A. Alim, M.A. Seitz and R.W. Hirthe, *J. Appl. Phys.*, **63**, 2337 (1988).
18. M.A. Alim, *J. Am. Ceram. Soc.*, **72**, 28 (1989).
19. R. Einzinger in Advances in Ceramics 1, Edited by L.M. Levinson (The American Ceramic Society, inc., Columbus, Ohio) 359-74 (1981).
20. T. Takemura, H. Kobayashi, Y. Takada and K. Sato, *J. Amer. Ceram. Soc.*, **69**, 430 (1986).
21. I.M. Hodge, M.D. Ingram and A.R. West, *J. Electroanal. Chem.*, **74**, 125 (1976).
22. J.T.S. Irvine, D.C. Sinclair and A.R. West, *Adv. Mater.*, **2**, 132 (1990).
23. International Centre for Diffraction Data, card 15-687.
24. *ibid*, card 34-1303.
25. M.A. Alim, M.A. Seitz and R.W. Hirthe, *J. Am. Cer. Soc.*, **71**, C52 (1988).
26. M.A. Alim and M.A. Seitz, *J. Am. Ceram. Soc.*, **71**, C246 (1988).
27. S.-N. Bai and T.-Y. Tseng, *J. of Electronic Materials*, **21**, 1073 (1992).
28. B.-S. Chiou and M.-C. Chung, *J. of Electronic Materials*, **20**, 885 (1991).
29. J. Lee, J.H. Hwang, I.J. Mashek, T.O. Mason, A.E. Miller and R.W. Siegel, *J. Mater. Res.*, **10**, 2295 (1995).
30. M. Matsuura and H. Yamaoki, *Jpn. J. Appl. Phys.*, **16**, 1261 (1977).
31. K. Al Abdullah, A. Bui and A. Lonbiere, *J. Appl. Phys.*, **69**, 4046 (1991).
32. F. Greuter, *Solid State Ionics*, **75**, 67 (1995).
33. G.D. Mahan, *J. Appl. Phys.*, **54**, 3825 (1983).
34. M. Bartkowiak, G.D. Mahan, F.A. Modine and M.A. Alim, *J. Appl. Phys.*, **79**, 273 (1996).
35. M. Tao, A. Bui, O. Dorlanne and A. Loubiere, *J. Appl. Phys.*, **61**(4), 1562 (1987).
36. G. Hohenberger and G. Tomandi, *J. Am. Ceram. Soc.*, **74**(9), 2067 (1991).
37. H.T. Sun, L.Y. Zhang and X. Yao, *J. Am. Ceram. Soc.*, **76**(5), 1150 (1993).
38. E. Olsson, R. Osterlund and G.L. Dunlop, in Ceramic Microstructures '86, eds. J.A. Pask and A.G. Evans, Plenum Press, New York 679–686 (1987).